Seismic activities and hazards of the seismic gaps in the Haiyuan fault in northeastern Tibet: Insights from numerical modelling earthquake interaction

Jianquan Chen[1], Chang Liu [1]*, Hang Zhang[1], Yaolin Shi[2]

1 State Key Laboratory of Marine Geology, Tongji University, Shanghai, China

2 Key Laboratory of Computational Geodynamics, Chinese Academy of Sciences, Beijing, China

* Corresponding author: Chang Liu (changliuu@tongji.edu.cn)

Highlights:

The 2022 Mw 6.6 Menyuan earthquake was delayed due to the stress shadow caused by historical earthquakes in northeastern Tibet.

The stress shadow covers the middle section of the Tianzhu Seismic Gap and prohibits its seismic activity.

The eastern portion of the Tianzhu Seismic Gap was stress loaded by historical earthquakes, indicating its increased seismic hazards.

Abstract: The 2022 Menyuan earthquake occurred in the Qilian-Haiyuan fault system in northeastern Tibet. To investigate the reason behind this earthquake and the seismic hazards of the Tianzhu Seismic Gap, we demonstrated the spatiotemporal stress variation on the fault system before and after 2022 through numerical modelling. We found that the 2022 earthquake was delayed due to a stress shadow caused by historical earthquakes. This stress shadow also covers the middle of the Tianzhu Seismic Gap and prohibits its seismic activities to some extent. Acting as a stress barrier to prevent the Tianzhu Seismic Gap rupturing in one event, this stress shadow may decrease the possibility of generating a future earthquake of magnitude more than Mw7.7 in this gap. The east portion of the Tianzhu Seismic Gap was stress loaded, indicating its increased seismic hazards. Attention should be paid to the hazards prevention in the eastern portion of the gap.

Plain Language Summary: The 2022 Mw 6.9 Menyuan earthquake occurred in the Qilian-Haiyuan fault system in northeastern Tibet. In this study, we demonstrated the space-time stress variation along the Qilian-Haiyuan fault system by calculating the stress change by several large earthquakes in the target region in the past century. We found a earthquake-induced stress shadow delayed the 2022 Menyuan earthquake. The seismic activities in the middle section of the Tianzhu Seismic Gap (to the east of the Qilian-Haiyuan fault system) are also prohibited by the this stress shadow. However, the east portion of the Tianzhu Seismic Gap was stress loaded by historical earthquake, indicating its increased seismic hazards. More attention should be paid to the future seismic hazards in the eastern portion of the Tianzhu Seismic Gap. It is helpful for hazards prevention and disaster relief for the government of Gansu province, China.

Keywords: The 2022 Menyuan earthquake, Tianzhu Seismic Gap, Haiyuan fault, Stress shadow, Stress trigger

1. Introduction

The west-east trending strike-slip Qilian-Haiyuan fault system locates in the northern margin of Qilian orogen in northeastern Tibet. It extends approximately 1000 km from the west near the Hala Lake to the east in Guyuan county in Gansu province, China (Yang et al., 2022). This fault system composes of several fault segments: the Hala Lake fault (HLHF), Tuolaishan fault (TLSF), Lenglongling fault (LLLF), Jinqianghe fault (JQHF), Maomaoshan fault (MMSF), Laohushan fault (LHSF), and Haiyuan fault (HYF) (Deng et al., 2007; Lasserre et al. 2002; Zheng et al., 2013; Yang et al., 2022) (Figure 1). The recent Mw 6.6 Menyuan earthquake with an epicenter of (37.828°N, 101.29°E) (the US Geological Survey [USGS]) occurred in this fault system on Jan 8, 2022, which caused damages to local high-speed rail lines (Peng et al., 2022; Yang et al., 2022) (Figure 1). Field investigations indicate that this earthquake produced a surface rupture of approximately 22 km (https://www.cea.gov.cn/cea/xwzx/fzjzyw/5646200/index.html). Aftershocks relocation and earthquake rupture modelling studies reveal that this earthquake ruptured both on the eastern and western portions of the TLSF and LLLF, respectively (Peng et al., 2022; Feng et al., 2022). The 2022 Menyuan earthquake located approximately 30–40 km west to another two earlier Menyuan earthquakes (the 1986 Mw 6.0 and 2016 Mw 5.9 thrust earthquakes in the Minyue-Damaying fault and north LLLF, respectively) (Zhang et al., 2020; Peng et al., 2022; Yang et al., 2022) (Figure 1). Peng et al. (2022) suggested that the 2022 Mw 6.6 Menyuan earthquake was likely promoted by the 2016 Mw 5.9 Menyuan earthquake due to the stress loaded on the 2022 earthquake rupture. However, the impact of the 1986 Mw 6.0 Menyuan earthquake on the 2022 Mw 6.6 Menyuan earthquake was neglected in the earthquake stress calculation by Peng et al. (2022). The reasons behind the 2022 Menyuan earthquake remain unknown.

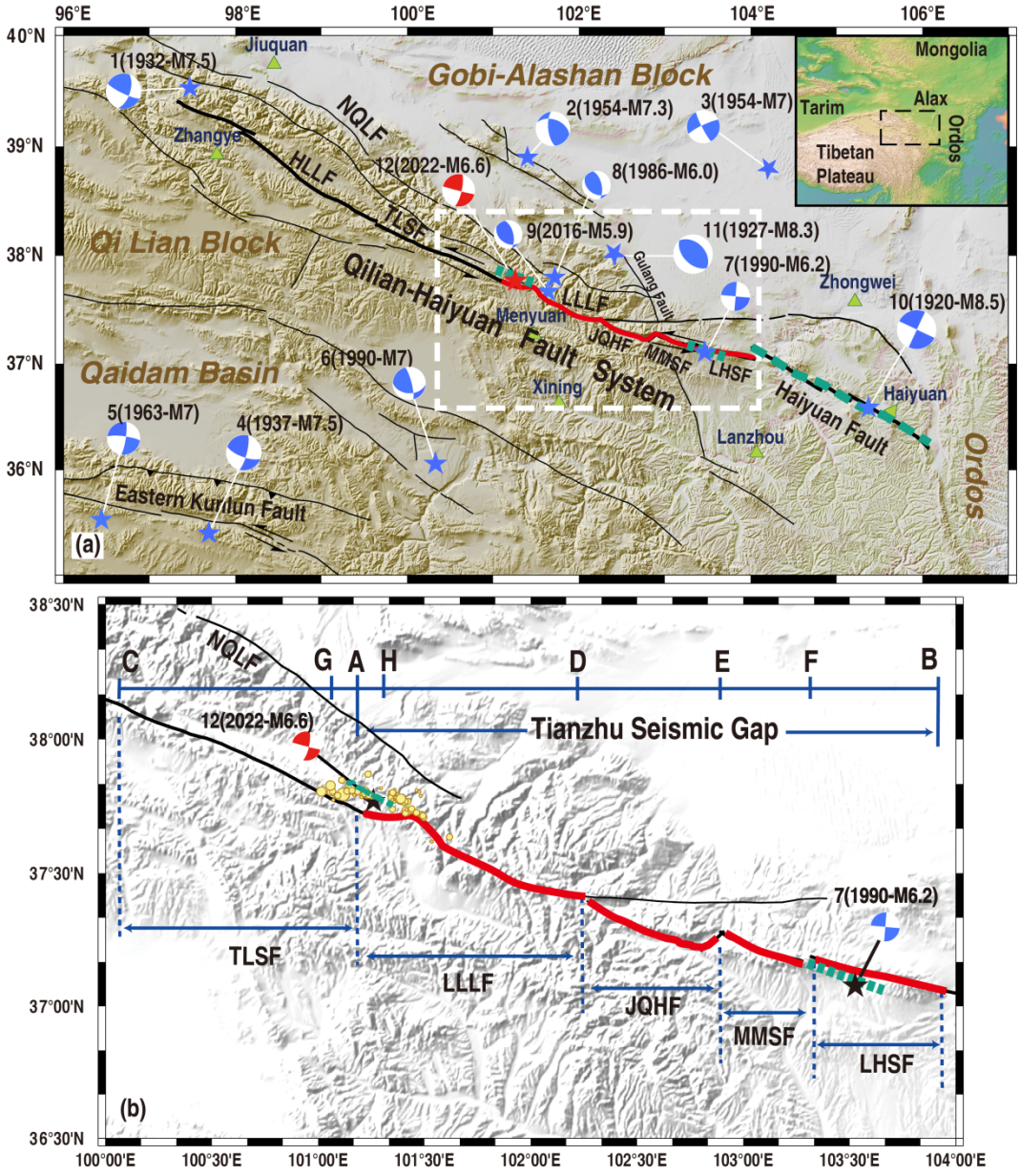

Figure 1: Geological setting of northeastern Tibet. (a) The blue stars illustrate the epicenters of 5 earthquakes (M 5.9, Nos. 7-10, and 12) and 7 earthquakes (M 7.0, Nos. 1-6 and 11) in and around the Qilian-Haiyuan fault system, respectively, from 1920 to 2022. The blue beach balls illustrate the focal mechanisms of 11 historical earthquakes (Nos. 1-11). The red star and beach ball illustrate the 2022 Mw 6.6 Menyuan earthquake (No. 12) epicenter and focal

mechanism, respectively. The earthquake parameters are summarized in Table S1 (Supporting Information Text S1). The black lines represent the active faults. The black and red solid bold lines present the Qilian-Haiyuan fault system and the Tianzhu Seismic Gap in this fault system, respectively. The bold green dashed lines represent the 1920 Mw 8.5 Haiyuan (No. 11) and 2022 Mw 6.6 Menyuan (No. 12) earthquakes ruptures. The light green triangles indicate the locations of cities with names. The upper right inset presents the location of the target area in a larger geological setting. (b) It illustrates the fault segments in the Tianzhu Seismic Gap in the area indicated by the white dashed line rectangle in (a). The yellow dots represent epicenters of the earthquakes ($M > 3.0$) from Jan 8, 2022 to Feb 8, 2021. HLHF: the Hala Lake fault; TLSF: the Tuolaishan fault; LLLF: the Lenglongling fault; JQHF: the Jinqianghe fault; MMSF: the Maomaoshan fault; LHSF: the Laohushan fault; HYF: the Haiyuan fault; NQLF: the north Qilian fault (Deng, 2007).

The 1920 Mw 8.5 Haiyuan ruptured the HYF segment (the eastern portion of the Qilian-Haiyuan fault system) by producing an approximately 230 km long surface rupture and caused more than 230,000 casualties based on the field investigation data (Liu-Zeng et al., 2007, 2015). After experiencing the recent 2022 earthquake and the 1920 Haiyuan earthquake, a seismic gap in the Qilian-Haiyuan fault system was left between these two earthquakes with the length of approximately 260 km, which was named as "Tianzhu Seismic Gap", including the LLLF, JQHF, MMSF, and LHSF (Gaudemer et al. 1995). This seismic gap has not experienced an earthquake of $M > 7.0$ for more than 800 years according to the historical earthquake documents (Gaudemer et al. 1995; Liu-Zeng et al., 2015; Xiong et al., 2018). So far the future seismic hazards of the Tianzhu Seismic Gap has been keeping unclear.

Earthquake interaction has significant influence on regional earthquake activities by increasing or decreasing Coulomb Failure Stress (ΔCFS) on target faults (Reasenberg and Simpson, 1992; Harris, 1998; Stein, 1999). Normally, earthquake activities are encouraged in the areas with increased stress, whereas earthquake activities are prohibited in the areas with decreased stress (Harris, 1998). This method has been successfully used in investigating the relation between main shock and aftershocks (King et al., 1994; Lin and Stein 2004; Toda et al., 2011), large earthquakes (Stein, 1999; King and Cocco, 2001; Stein 2003; Freed, 2005), and volcanoes and earthquakes (Nostro et al., 1998; Lara et al., 2004; Walter et al., 2005; Walter and Amelung, 2007; Eggert and Walter, 2009). Historical earthquake catalogue indicates that several large earthquake (M 7.0) occurred in and around the Qilian-Haiyuan fault system in northeastern Tibet during the past century. Taken as an example, the 1927 Mw 8.3 Gulang earthquake (No. 11 in Fgure1) rupture locates less than several tens of kilometers north to the Qilian-Haiyuan fault system (Deng et al., 2007, Xiao and He et al., 2015). This earthquake might have significant impact on the seismic activity of the Qilian-Haiyuan fault system due to its large magnitude and proximity. However, the stress transferred to the this fault system by those historical large earthquakes, as well as its influence on the 2022 Menyuan earthquake and the

seismic activities and hazards of the Tianzhu Seismic Gap has not been well studied.

To investigate those questions above, we simulated the ΔCFS induced by 12 large historical earthquakes with available focal mechanisms in and around the Qilian-Haiyuan fault system during the period from 1920 to 2022 in this study. Space-time stress distributions before and after 2022 along the Qilian-Haiyuan fault system were evaluated to determine its control on the 2022 Menyuan earthquake, as well as their influence on the seismic activities and hazards of the Tianzhu Seismic Gap. This is important for understanding the reasons for earthquake generation and migration in the northeastern Tibet from the perspective of earthquake interaction, and also helpful for hazards prevention and disaster relief for the government of Gansu province, China.

2. Historical earthquakes

Together with the Altyn Tagh, Ganzi-Yushu-Xianshuhe, and Kunlun faults, the Qilian-Hiayuan fault system consists of the tectonic boundaries of the north and northeastern Tibet (Peltzer et al., 1988; Tapponnier et al., 2001). With the continuing south-north convergence between India and Eurasia plates, deformation along these major boundary strike-slip faults accommodates the eastward extrusion of the Tibetan Plateau by generating frequent large earthquakes in northeastern Tibet (Meyer et al., 1998; Wang et al., 2001). Geodetic data indicates that slip rates vary along the approximately 1000 km long Qilian-Haiyuan fault system, which are 1-2 mm/a, 4-6 mm/a, 3.4-6.4mm/a, 2.9-5.6mm/a, and 5 mm/a on the HLHF; TLSF; LLLF; JQHF-MMSF-LHSF, and HYF , respectively (Wang et al., 2020).

During the past century, the eastern Qilian-Haiyuan fault system generated 5 large earthquakes (M 5.9): 1990 Mw 6.2 Tianzhu (No. 7), 1986 Mw 6.0 Menyuan (No. 8), 2016 Mw 5.9 Menyuan (No. 9), 1920 Mw 8.5 (No. 10) Haiyuan, and 2022 Mw 6.6 Menyuan earthquakes (No. 12) (Tang and Wang, 1993; Liu-Zeng et al., 2007, 2015; Zhang et al., 2020; Peng et al., 2021; Yang et al., 2022). According to historical earthquake document, 7 historical large earthquake (M 7.0) occurred within the horizontal distance of less than 300 km from the Qilian-Haiyuan fault system from 1920 to 2022. This includes the 1932 Mw 7.5 Changma (No. 1), 1954 Mw 7.3 Shandan (No. 2), 1954 Mw 7.0 Minqin (No. 3), 1937 Tuosuo Lake (No. 4), 1963 Alake Lake (No. 5), 1990 Mw 7.0 Gonghe (No. 6), and 1927 Mw 8.5 Gulang earthquakes (Nos. 11) (Molnar and Deng, 1984; Gaudemer et al., 1995; Liu and Fu, 2001; Wan et al., 2007; Xu et al., 2002) (Figure 1). The detailed earthquake parameters are summarized in Table S1 (Supporting Information Text S1). In total, 12 historical earthquakes (Nos. 1-12 in Figure 1) were included in the ΔCFS calculations in this study.

3. Stress results

We calculate the combined ΔCFS before and after the 2022 Mw 6.6 Menyuan earthquake, caused by 12 historical earthquakes in and around the Qilian-Haiyuan fault system from 1920 to 2022. The calculated ΔCFS includes

contributions from the co-seismic stress changes and postseismic stress relaxation. The viscosities of the middle and lower crusts and the mantle can be found in Table S2 (Supporting Information Text S2), and more details of the visco-elastic model can be found in the Supporting Information.

3.1. Stress evolution before and after 2022

3.1.1. Stress change before the 2022 Menyuan earthquake

In this section the ΔCFS was calculated at a 10-km depth (close to the hypocenter depth for the 2022 Menyuan earthquake suggested by USGS) with receiver faults identical to the focal mechanism (strike = 104°, dip = 88°, rake = 15°) of the 2022 Menyuan earthquake (USGSa) induced by 11 historical earthquakes.

Figures 2(a)–2(k) presents the ΔCFS map at a 10-km depth before 2022 individually induced by 11 large earthquakes (Nos. 1–11). Figures 3(a)–3(k) presents the ΔCFS along the Qilian-Haiyuan fault system at a 10-km depth before 2022 individually induced by 11 large earthquakes (Nos. 1–11). All the 11 historical earthquakes increased stress before 2022 in the 2022 Menyuan earthquake rupture zone (segment GH in Figure 3) except for three of them (the 1963 Mw 7.0 Alake Lake earthquake [No. 5], 1986 Mw 6.0 Menyuan earthquake [No. 8], and the 1927 Gulang Mw 8.3 earthquake [No. 11]). The ΔCFS on the 2022 Menyuan earthquake hypocenter before 2022 was changed by -2.886 kPa, 0.208 kPa, 3.957 kPa, and -18.44 kPa by the 1986 Mw 6.0 Menyuan (No. 8), 2016 Mw 5.9 Menyuan (No. 9), 1920 Mw 8.5 Haiyuan (No. 10), and 1927 Mw 8.3 Gulang (No. 11) earthquakes, respectively (Figures 2 and 3). The stress change on the 2022 Menyuan earthquake hypocenter by the other seven earthquakes (Nos. 1–7) was negligible owing to the limited ΔCFS values (between -0.01 kPa and 0.02 kPa) (Figures 2 and 3).

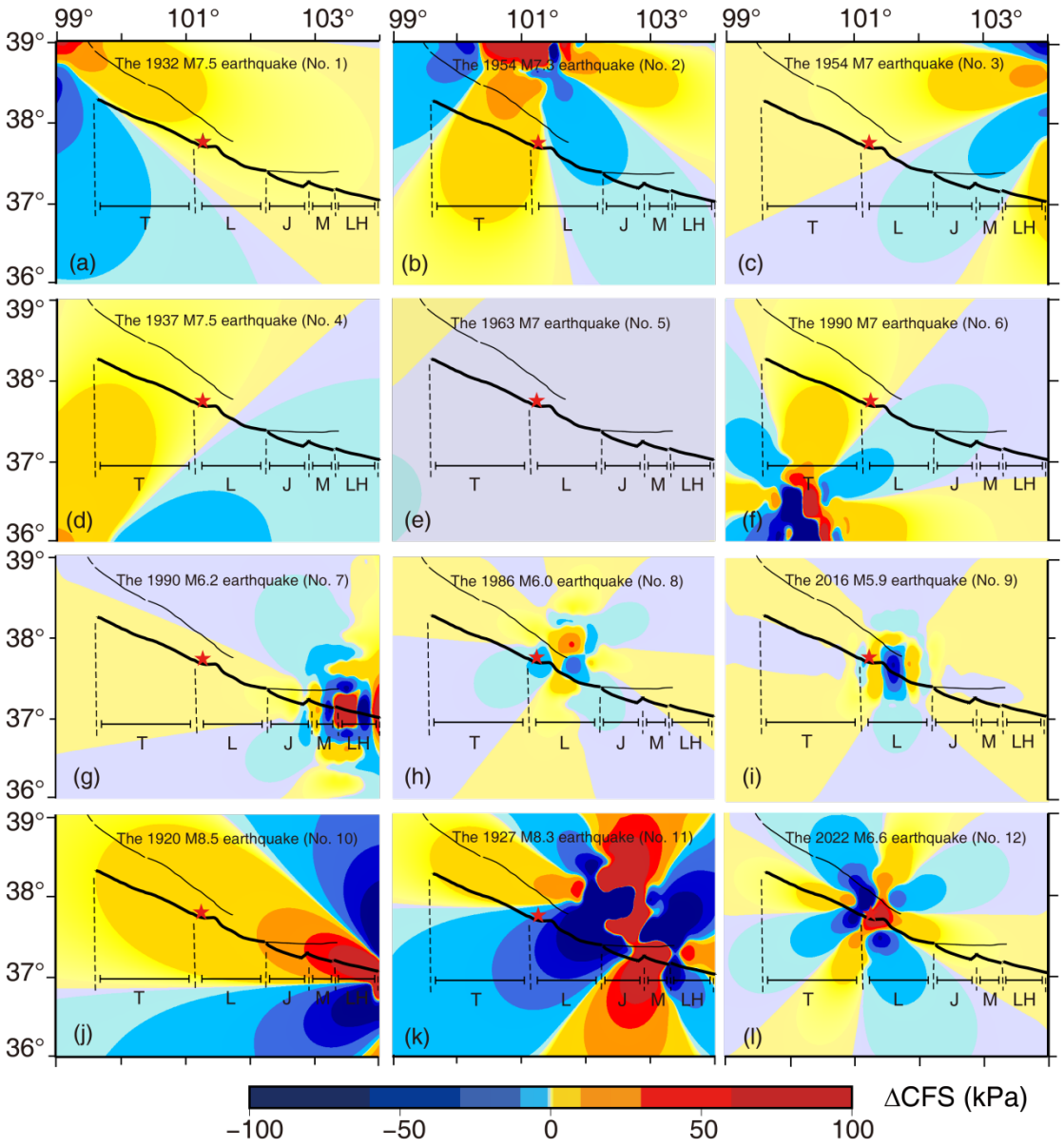

Figure 2: ΔCFS map at a 10-km depth before 2022 induced by: (a) the 1932 Mw 7.5 Changma earthquake (No. 1), (b) the 1954 Mw 7.3 Shandan earthquake (No. 2), (c) the 1954 Mw 7.0 Minqin earthquake (No. 3), (d) the 1937 Tuosuo Lake earthquake (No. 4), (e) the 1963 Alake Lake earthquake (No. 5), (f) the 1990 Mw 7.0 Gonghe earthquake (No. 6), (g) the 1990 Mw 6.2 Tianzhu earthquake (No. 7), (h) the 1986 Mw 6.0 Menyuan earthquake (No. 8), (i) the 2016 Mw 5.9 Menyuan earthquake (No. 9), (j) the 1920 Mw 8.5 Haiyuan

earthquake (No. 10), and (k) 1927 Mw 8.3 Gulang earthquake (No. 11); (l) ΔCFS map at a 10-km depth just after 2022 induced by the 2022 Mw 6.6 Menyuan earthquake (No. 12). The black curved lines represent the faults, and the epicenter of the 2022 Menyuan earthquake is marked with a red star. T: the Tuolaishan fault; L: the Lenglongling fault; J: the Jinqianghe fault; M: the Maomaoshan fault; LH: the Laohushan fault; H: the Haiyuan fault.

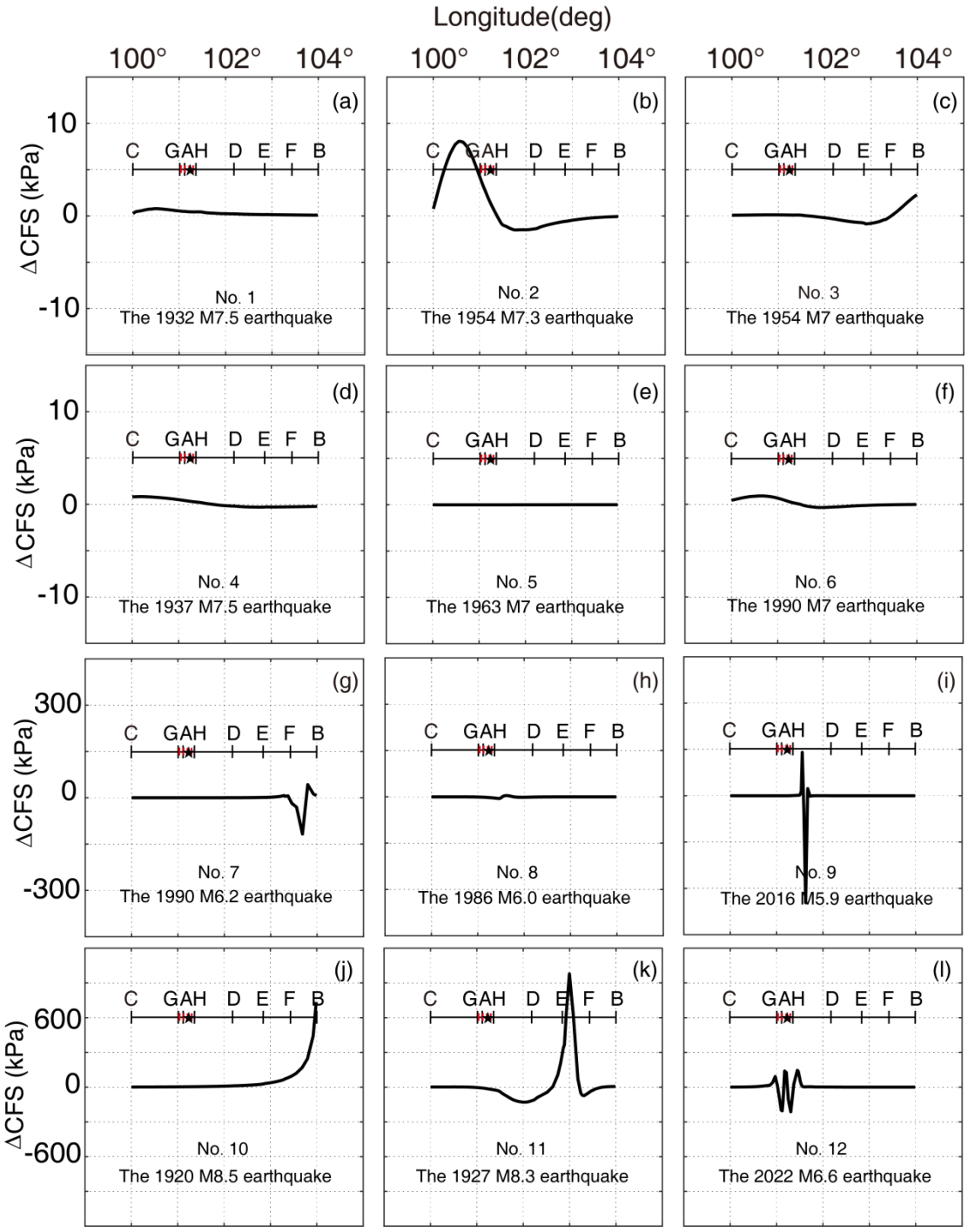

Figure 3: ΔCFS along the Qilian-Haiyuan fault system at a 10-km depth

before 2022 induced by: (a) the 1932 Mw 7.5 Changma earthquake (No. 1), (b) the 1954 Mw 7.3 Shandan earthquake (No. 2), (c) the 1954 Mw 7.0 Minqin earthquake (No. 3), (d) the 1937 Tuosuo Lake earthquake (No. 4), (e) the 1963 Alake Lake earthquake (No. 5), (f) the 1990 Mw 7.0 Gonghe earthquake (No. 6), (g) the 1990 Mw 6.2 Tianzhu earthquake (No. 7), (h) the 1986 Mw 6.0 Menyuan earthquake (No. 8), (i) the 2016 Mw 5.9 Menyuan earthquake (No. 9), (j) the 1920 Mw 8.5 Haiyuan earthquake (No. 10), and (k) 1927 Mw 7.9–8.3 Gulang earthquake (No. 11); (l) ΔCFS along the Qilian-Haiyuan fault system at a 10-km depth just after 2022 based on the 2022 Mw 6.6 Menyuan earthquake (No. 12). The red dashed line indicates the 2022 earthquake rupture (segment GH) on the Qilian-Haiyuan fault system (segment BC). The longitude of the 2022 Menyuan earthquake epicenter is marked with a black star. Segments AD, DE, EF, and FB indicate the LLLF, JQHF, MMSF, and LHSF, respectively, in the Tianzhu Seismic Gap (segment AB).

Figure 4 (a) presents the cumulative ΔCFS map at a 10-km depth before 2022 induced by 11 large historical earthquakes (Nos. 1–11). Figure 5 (a) illustrates the cumulative ΔCFS distribution along the Qilian-Haiyuan fault system resulting from these 11 earthquakes. The stress before 2022 was unloaded in the 2022 Menyuan earthquake rupture zone (segment GH in Figures 4 (a) and 5). An ΔCFS decrease of about -15.38 kPa was observed at the 2022 Menyuan earthquake hypocenter. This unloaded stress was mainly controlled by the 1927 Mw 8.3 Gulang earthquake (-18.44 kPa) (No. 11) by comparing Figure 5 (a) with Figure 3.

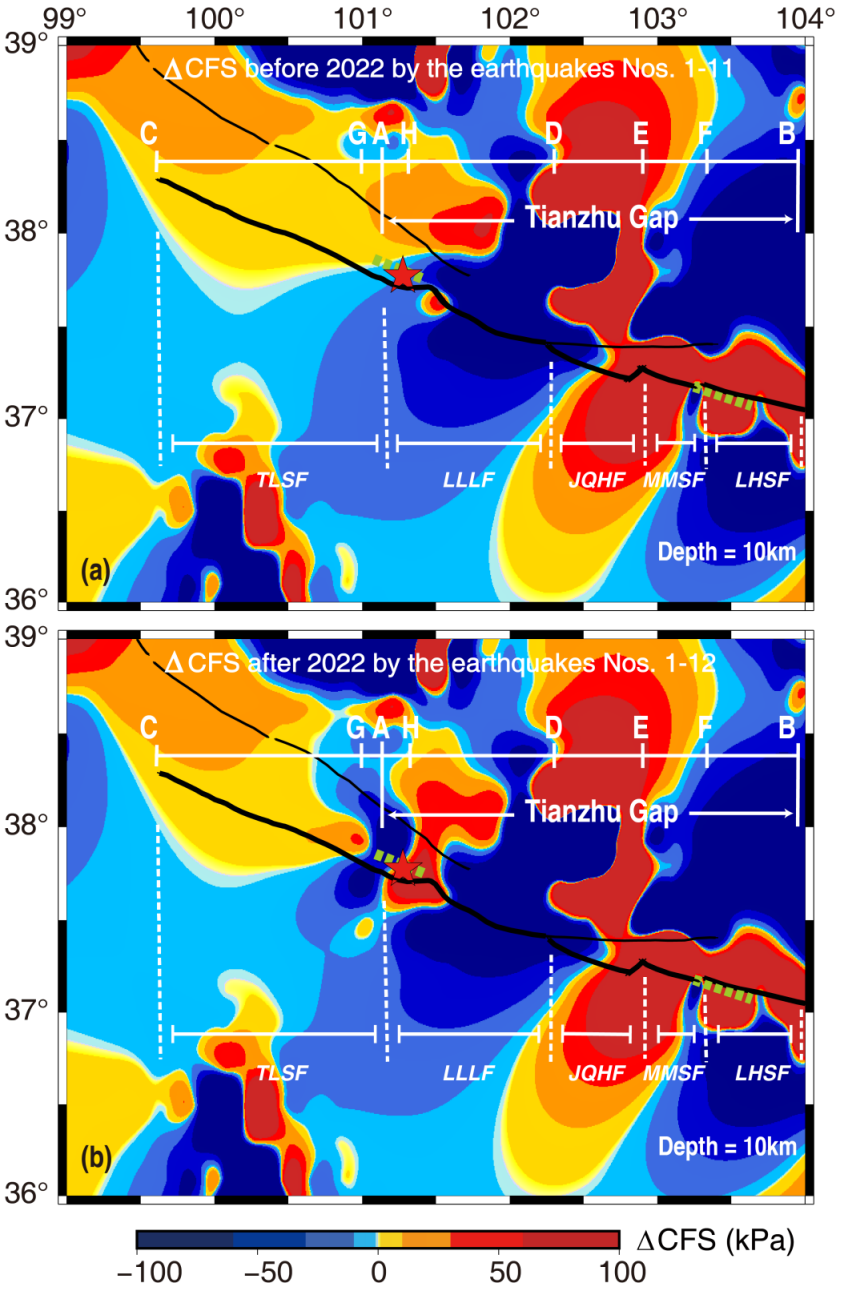

Figure 4: Cumulative ΔCFS map at a 10-km depth (a) before 2022 caused by 11 earthquakes (Nos. 1–11) and (b) just after 2022 caused by 12 earthquakes (Nos. 1–12) including the 2022 Mw 6.6 Menyuan earthquake. The faults are represented by black curved lines, and the epicenter of the 2022 Maduo earth-

quake is marked with a red star. The green dashed lines indicate the 1990 Mw 6.2 Tianzhu and 2022 Mw 6.6 Menyuan earthquakes ruptures on the Qilian-Haiyuan fault system (segment BC). TLSF: the Tuolaishan fault; LLLF: the Lenglongling fault; JQHF: the Jinqianghe fault; MMSF: the Maomaoshan fault; LHSF: the Laohushan fault; HYF: the Haiyuan fault.

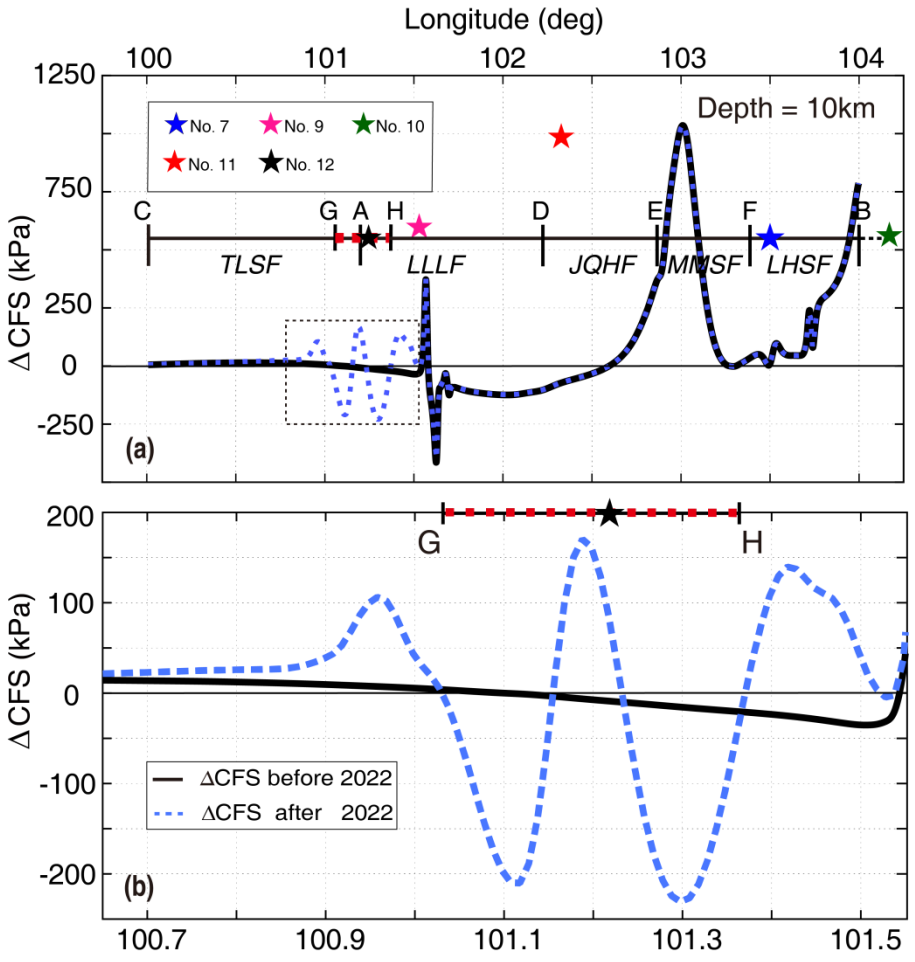

Figure 5: **(a)** Cumulative ΔCFS along the Qilian-Haiyuan fault system at a 10-km depth before 2022 caused by 11 earthquakes (Nos. 1–11) and just after 2022 caused by 12 earthquakes (Nos. 1–12). The red dashed line indicates the 2022 Mw 6.6 Menyuan earthquake rupture (segment GH) on the Qilian-Haiyuan fault system (segment BC). The longitudes of the 1990 Mw 6.2 Tianzhu (No. 7), 2016 Mw 5.9 Menyuan (No. 9), 1920 Mw 8.5 Haiyuan (No. 10), 1927 Mw 8.3 Gulang (No. 11), and 2022 Mw 6.6 Menyuan (No. 12) earthquakes epicenters are marked with blue, pink, green, red, and black stars, respectively. (b) The details of ΔCFS in the 2022 Menyuan earthquake rupture area are indicated by

a black dashed line rectangle in (a).

3.1.2. Stress change during the 2022 Menyuan earthquake

Figure 2(l) presents the co-seismic ΔCFS map at a 10-km depth induced by the 2022 Mw 6.6 Menyuan earthquake (No. 12), and Figure 3(l) details the co-seismic ΔCFS variation along the Qilian-Haiyuan fault system at a 10-km depth induced by this event. The stress in most areas of the earthquake rupture zone was released in a 10-km depth with a maximum ΔCFS value of approximately -230 kPa during the 2022 Menyuan earthquake (Figure 3(l)). The maximum co-seismic stress release reached -921.35 kPa at a 5-km depth (Figure S1(b) and Table S3 in Supporting Information Text S3). However, the stress was promoted by 106 kPa and 145 kPa to the western and eastern ends of the earthquake rupture at a 10-km depth (segment GH in Figure 3(l)), respectively.

3.1.3. Stress change after the 2022 Menyuan earthquake

Figure 4(b) illustrates the cumulative ΔCFS map at a 10-km depth after 2022 induced by 12 historical earthquakes including the 2022 Menyuan earthquake. Figure 5(a) illustrates the ΔCFS distribution along the Qilian-Haiyuan fault system at a 10-km depth after 2022 due to these 12 earthquakes. Except stress perturbation in the 2022 Menyuan earthquake rupture zone (segment GH in Figure 5) induced by this event, stress on the other segments of the Tianzhu Seismic Gap was almost unchanged before and after 2022 (Figure 5).

The stress was loaded in the segment (with the length of approximately 18 km) between the 2016 Mw 5.9 (No. 9) and 2022 Mw 6.6 (No. 12) Menyuan earthquakes with a peak value of 375.15 kPa (Figure 5(a)) in the western portion of the LLLF (segment AD in Figure 5(a)). However, the stress in the eastern portion (with the length of approximately 50 km) of the LLLF located in a stress shadow with a maximum ΔCFS decrease of -396.24 kPa. This stress shadow was mainly controlled by the 2016 Mw 5.9 Menyuan (-335 kPa) (No.9) and 1927 Mw 8.3 Gulang (No. 11) earthquakes by comparing Figure 5 (a) with Figure 3.

The western portion (with the length of approximately 30 km) of JQHF (segment DE in Figures 4 (b) and 5(a)) also located in a stress shadow with a maximum ΔCFS decrease of -101.18 kPa at its western end. This stress shadow was mainly controlled by the 1927 Mw 8.3 Gulang earthquake (-111.4 kPa) (No. 12) by comparing Figure 5 (a) with Figure 3. However, The eastern portion (with the length of approximately 35 km) of JQHF was stress loaded with a maximum value of 216.7 kPa at its eastern end, which was mainly contributed by the 1920 Mw 8.5 Haiyuan (No. 10) and 1927 Mw 8.3 Gulang earthquake (192.5 kPa) (No. 11) by comparing Figure 5 (a) with Figure 3.

The stress was loaded in the entire MMSF (with the length of approximately 54 km) (segment EF in Figures 4 (b) and 5(a)) with a peak value of 1035 kPa except for its very eastern tip with a minor stress decrease of -1.53 kPa (Figures 4 (b) and 5(a)). The increased stress on the MMSF was mainly controlled by 1920 Mw 8.5 Haiyuan (No. 10) and the 1927 Mw 8.3 Gulang (No. 11) (996.1

kPa) earthquakes by comparing Figure 5 (a) with Figure 3.

The stress was loaded in the entire LHSF (with the length of approximately 60 km) (segment FB in Figures 4 (b) and 5(a)) with a peak value of 786.68 kPa at its eastern end. The increased stress on this fault segment was mainly controlled by the 1920 Mw 8.5 Haiyuan (No. 10) (772 kPa) earthquake by comparing Figure 5 (a) with Figure 3.

3.2. Stress variation with depth before and after 2022

The cumulative ΔCFS distribution along the Tianzhu Seismic Gap at different depths induced by 12 historical earthquakes before 2022 and after 2022 is presented in Figures S1 (Supporting Information Text S3). Tables S3 (Supporting Information Text S3) summarizes the cumulative ΔCFS at different locations along the Tianzhu Seismic Gap at different depths before and after 2022. The stress pattern at different depths along the Tianzhu Seismic Gap was similar, while the stress values significantly changed. Taken as an example, varying depth from 5 km to 20 km changed the ΔCFS from -15.627 kPa to -11.914 kPa at the 2022 Menyuan earthquake hypocenter before 2022 (Figure S1a) (Table S3). The maximum ΔCFS increase after 2022 varied between 592.71 kPa and 1180 kPa and between 580.73 kPa and 1138.8 kPa in the MMSF (segment EF in Figure S1) and LHSF (segment FB in Figure S1), respectively, by varying depth from 5 km to 20 km (Table S3 in Supporting Information).

3.3. Sensitivity of Stress

We varied only one model parameter to investigate the sensitivity of stress results for each case, such that all other parameters remained constant based on the above model setting for the following calculation. The parameters that were varied include the 1920 Mw 8.5 Haiyuan (No. 10) and 1927 Mw 8.3 Gulang (No. 11) earthquakes source parameters, the strike, dip, and rake angles of the Tianzhu Seismic Gap, frictional coefficient ', and the viscosities of the middle and lower crusts. By considering the uncertainty from all the cases by model parameterization, including the 1920 Haiyuan and 1927 Gulang earthquakes source parameters and the receiver fault parameters, we found that the ΔCFS before 2022 ranged from -27.49 kPa to -1.07 kPa at the 2022 Menyuan earthquake hypocenter. The minimum ΔCFS decrease after 2022 ranged from -430.84 kPa to -342.14 kPa and from -184.29 kPa to -18.14 kPa in the eastern LLLF and western JQFH, respectively. The maximum ΔCFS increase after 2022 ranged from 229.90 kPa to 562.58 kPa, from 10.66 kPa to 655.50 kPa, from 419.86 kPa to 3359.4 kPa, and from 516.55 kPa to 1755 kPa in the western LLLF (between the 2016 Mw 5.9 [No. 9] and 2022 Mw 6.6 [No.12] Menyuan earthquakes), eastern JQHF, MMSF, and LHSF, respectively (Text S4 in Supporting Information).

4. Discussions

4.1. The delayed 2022 Menyuan earthquake

In order to investigate the relation between the three Menyuan earthquakes: the

1986 (Mw 6.0) (No. 8), 2016 (Mw 5.9) (No. 9), and 2022 Mw 6.6 (No. 12) earthquakes, we demonstrated the stress change on the 2022 Menyuan earthquake rupture induced by the 1986 and 2016 Menyuan earthquakes before 2022. We found that the 1986 earthquake decreased the ΔCFS of -2.886 kPa on the 2022 earthquake hypocenter. However, the 2016 earthquake increased the ΔCFS of 0.208 kPa on the 2022 earthquake hypocenter, which supports the previous proposal by Peng et al. (2022) that the 2022 earthquake was triggered by the 2016 earthquake due to stress loading on the 2022 earthquake rupture.

However, the entire 2022 Menyuan earthquake rupture located in a stress shadow with a negative stress (before 2022) of -15.38 kPa on the 2022 Menyuan earthquake hypocenter by considering the cumulative ΔCFS resulting from 11 historical earthquakes (Nos. 1-11) during the period from 1920 to 2022. Generally, earthquake activity in stress shadow zone is prohibited by unloaded stress from the perspective of earthquake interaction (Mallman and Parsons, 2008). This method has been successfully used to investigate the role of earthquake-induced negative stress on the decreased seismic activities related to the 1857 Fort Tejon and 1906 San Francisco earthquakes in the San Andreas Fault system (Simpson et al., 1988; Harris and Simpson, 1996; Harris, 1998; Freed and Lin, 2001; Mallman and Parsons, 2008) and low seismicity in the Bhutan Himalaya (Gahalaut et al., 2011). Based on this finding, we suggest that the 2022 Menyuan earthquake was delayed because of the unloaded stress on the earthquake rupture resulting from historical earthquakes interactions in northeastern Tibet during the past century. By comparing the stress change on the 2022 Menyuan earthquake hypocenter individually by 11 historical earthquake (Nos 1-11), we found that this stress shadow was mainly controlled by the 1927 Mw 8.3 Gulang earthquake.

4.2. Future hazards on the Tianzhu Seismic Gap

Our results demonstrate strong stress contrast among different fault segments in the Tianzhu Seismic Gap (Figure 5) after 2022, which was mainly controlled by five historical earthquakes: the 1990 Mw 6.2 Tianzhu (No. 7), 2016 Mw 5.9 Menyuan (No. 9), 1920 Mw 8.5 Haiyuan (No. 10), 1927 Mw 8.3 Gulang (No. 11), and 2022 Mw 6.6 Menyuan (No.12) earthquakes.

Stress increase was observed in the segment (with the length of approximately 18 km) between the 2016 Mw 5.9 (No. 9) and 2022 Mw 6.6 (No. 12) Menyuan earthquakes with the peak ΔCFS value of approximately 375.15 kPa in the western portion of the Tianzhu Seismic Gap. This stress value (375.15 kPa) is much higher than the typical stress threshold of 10 kPa (Reasenberg and Simpson, 1992), indicating its increased seismic hazards.

The eastern portion of the Tianzhu Seismic Gap (starting from the middle of the JQHF to the east end of the LHSF with the length of approximately 149 km) was also stress loaded due to the 1920 Mw 8.5 Haiyuan (No. 10) and 1927 Mw 8.3 Gulang (No. 11) earthquakes (Figures 4 and 5). The peak value of the increased ΔCFS in the LHSF (with the length of approximately 60 km),

MMSF (with the length of approximately 54 km), and eastern portion (with the length of approximately 35 km) of the JQHF were approximate 786.68 kPa, 1035 kPa, and 216.7 kPa, respectively. These stress values are much higher than the typical stress threshold of 10 kPa (Reasenberg and Simpson, 1992), suggesting increased seismic hazards potential in the eastern Tianzhu Seismic Gap. Our stress results are sensitive to the model parameters. By considering the uncertainty from all cases by model parameterization (see Section 4.1), we found that the maximum ΔCFS increase after 2022 ranged from 516.55 kPa to 1755 kPa, from 419.86 kPa to 3359.4 kPa, and from 10.66 kPa to 655.50 kPa, in the LHSF, MMSF, and eastern JQHF, respectively. Compared with a typical stress release of 1000–2000 kPa for small and medium earthquake and approximately 5000 kPa for large earthquakes (Zielke and Arrowsmith 2008), the loaded stress with these values are large enough to bring those fault segments close to their failure criteria. Although the 1990 Mw 6.2 Tianzhu earthquake did occurred in the west of the LHSF, this earthquake was not large enough to fully release the accumulated energy in the LHSF due to its relatively low magnitude (Mw 6.2) and limited rupture length of f approximately 20 (Liu-Zeng et al., 2007). If the whole eastern portion of the Tianzhu Seismic Gap (with the length of approximately 149 km, including the eastern JQFH, MMSF, and LSHF) ruptures, there might be a future earthquake with a magnitude greater than 7.4, thus releasing accumulated energy at a fault slip rate close to approximately 4–6 mm/a over the past centuries (Wang et al., 2020). Furthermore, paleoearthquake investigations have suggested that this seismic gap has not experienced an earthquake of $M > 7.0$ for more than 800 years according to the historical earthquake documents (Gaudemer et al. 1995; Liu-Zeng et al., 2015; Wang et al. 2017; Xiong et al., 2018). Subsequently, more attention should be paid to the east portion of the Tianzhu Seismic Gap.

Note that these two stress increased zones in the Tianzhu Seismic Gap mentioned above are separated by a stress shadow zone (starting from the east of the 2016 Mw 5.9 (No. 8) to the middle of the JQHF) with the maximum ΔCFS decrease of -396.24 kPa. This stress shadow with relatively large negative ΔCFS value may act as a stress barrier to prohibit the future earthquake in this fault segment to some extent from the perspective of fault interaction (Mallman and Parsons, 2008). By preventing the whole Tianzhu Seismic Gap being ruptured in one event, it may consequently decrease the possibility of generating a future large earthquake of magnitude more than Mw 7.7 in Tianzhu Seismic Gap. The role of stress shadows on limiting earthquake rupture extent is not unique in the Tianzhu Seismic Gap of the Qilian-Haiyuan fault system. This phenomenon was also previously observed in some other earthquake zones, such as the northeast unilateral rupture of the 2008 Mw 7.9 Wenchuan earthquake in eastern Tibet (Liu et al., 2018, 2020), and the limitation of the 2018 Mw 7.5 Palu earthquake rupture extent in the Palu-Koro fault in Central Sulawesi, Indonesia (Liu et al., 2021).

Our findings of stress shadow in the middle of the Tianzhu Seimic Gap are congruent with those of Xiong et al. (2018) who calculated the ΔCFS of the

Tianzhu Seismic Gap caused by 5 historical earthquakes (M>7.0) around the Qilain-Haiyuan fault system. However, the contribution by each historical event to the stress change on different fault segments in the Tianzhu Seismic Gap was not clear by Xiong et al. (2018). By comparing the stress change individually by 12 historical events (Nos. 1-12) (Figures 2 and 3), we found that the stress shadow zone in the eastern LLLF and the western JQHF are mainly controlled the 1927 Mw 8.3 Gulang (No. 11) and 2016 Mw 6.6 Menyuan (No. 9) earthquake. Note that the maximum ΔCFS decrease of -396.24 kPa in this stress shadow zone suggested in this study is much lower than the estimates of -190 kPa by Xiong et al. (2018). Our results show that the 2016 Mw 6.6 Menyuan (No. 9) earthquake had the major contribution to the stress show by decreasing ΔCFS with the peak value of -335 kPa on the LLLF. However, this contribution by the 2016 Mw 6.6 Menyuan earthquake (No. 9) was neglected by Xiong et al. (2018), since this earthquake was excluded in the earthquake catalogue use in his ΔCFS calculation. This is the reason for why the maximum ΔCFS decrease of -396.24 kPa in the eastern LLLF estimated in this study is much lower than that of -190 kPa by Xiong et al. (2018). It also indicates that it is important to use a complete earthquake catalogue when estimating the seismic hazards in the Tianzhu Seismic Gap by calculating earthquake-induced stress change.

5. Conclusions

To investigate the reason behind the 2022 Menyuan earthquake and the seismic hazards of the Tianzhu Seismic Gap from the perspective of earthquake interaction, we simulated the ΔCFS on the Qilian-Haiyuan fault system by several historical earthquakes in the past century. By demonstrating the spatiotemporal stress variation along the Tianzhu Seismic Gap before and after 2022, we reached the following conclusions:

(1) There is a strong stress contrast among different fault segments in the Tianzhu Seismic Gap, which is mainly controlled by 5 historical earthquakes: the 1920 Mw 8.5 Haiyuan, 1927 Mw 7.3 Gulang, 1990 Mw 6.2 Tianzhu, 2016 Mw 5.9 Menyuan, and 2022 Mw 6.6 Menyuan earthquakes.

(2) The 2022 Mw 6.6 Menyuan earthquake was delayed due to the stress shadow in the earthquake rupture caused by the 1927 Mw 8.3 Gulang earthquake.

(3) The stress shadow also covers the fault segment starting from the east of the 2016 Mw 5.9 earthquake to the middle of the JQHF, which may prohibit the future seismic activity in this fault segment to some extent. By acting as a stress barrier to prevent the whole Tianzhu Seismic Gap being ruptured in one event, it consequently may decrease the possibility of generating a future earthquake of magnitude more than M 7.7 in the Tianzhu Seismic Gap.

(4) The east portion of the Tianzhu Seismic Gap starting from the middle of the JQHF to the east end of the LHSF was also stress loaded due to the 1920 Mw 8.5 Haiyuan and 1927 Mw 8.3 Gulang earthquakes, indicating its increased seismic hazards. More attention should be paid to the future hazards prevention

in the east portion of the Tianzhu Seismic Gap, including the eastern portion of the JQHF, MMSF, and LHSF.

Acknowledgements:

This research was supported by the National Natural Science Foundation of China (Nos. 41974102, U1839207). The earthquake data used in this study is available at "zenodo" (https://zenodo.org/record/6397292).

References

Chen,W. P., and P.Molnar (1977), Seismicmoments ofmajor earthquakes and average rate of slip in central Asia, J. Geophys. Res., 82,2954–2969

Clark, M. K., Bush, J. W., & Royden, L. H. (2005). Dynamic topography produced by lower crustal flow against rheological strength heterogeneities bordering the Tibetan Plateau. Geophysical Journal International, 162(2), 575–590.

Deng Qi-dong Ran Yong-kang YANG Xiao-ping et al 2007 Active Tectonic Map of China. Seismological Press Beijing(in Chinese).

Eggert S., T. R. Walter, 2009. Volcanic activity before and after large tectonic earthquakes: observations and statistical significance, Tectonophysics, 471: 14-26.

Feng, W., He, X., Zhang, Y., et al.,. Seismic faults of the 2022 Mw6.6 Menyuan, Qinghai earthquake and its implication for the regional seismogenic structures. 2022

Freed A. M., 2005. Earthquake triggering by static, dynamic, and postseismic stress transfer, Annual Review Earth Planetary Sciences, 33: 335-367.

Guo, P., Han, Z.J., Jiang, W.L., Mao, Z.B., 2017. Holocene left-lateral slip rate of theLenglongling fault, northeastern margin of the Tibetan Plateau (in Chinese). Seismol. Geol. 39 (2), 323–341.

Gaudemer, Y., Tapponnier, P., Meyer, B., Peltzer, G., Shunmin, G., Zhitai, C., Huagung, D., & Cifuentes, I. (1995). Partitioning of crustal slip between linked, active faults in the eastern Qilian Shan, and evidence for a major seismic gap, the 'Tianzhu gap', on the western Haiyuan Fault, Gansu (China). Geophysical Journal International, 120(3), 599–645. https://doi.org/10.1111/j.1365-246X.1995.tb01842.x

Gahalaut, V., Rajput, S.,&Kundu, B. (2011).Low seismicity in the Bhutan Himalaya and the stress shadow of the 1897 Shillong Plateau earthquake. Physics of the Earth and Planetary Interiors, 186(3), 97-102.

Hilley, G.E., Blisniuk, P.M. & Strecker, M.R., 2005. Mechanics anderosion of basement-cored uplift provinces, J. geophys. Res., 110, doi:10.1029/2005JB003704.

Harris, R. A. (1998), Introduction to special section: Stress triggers, stress shadows, and implications for seismic hazard, J. Geophys. Res., 103, 24,347–24,358.

King G. C., R. S. Stein, J. Lin, 1994. Static stress changes and the triggering of earthquakes, Bulletin of the Seismological Society of America, 84: 935-953.

King G., M. Cocco, 2001. Fault interaction by elastic stress changes: New clues from earthquake sequences, in Advances in Geophysics, Elsevier, 1-VIII.

Lara L., J. Naranjo, H. Moreno, 2004. Rhyodacitic fissure eruption in Southern Andes (Cordón Caulle; 40.5 S) after the 1960 (Mw 9.5) Chilean earthquake: a structural interpretation, Journal of Volcanology and Geothermal Research, 138: 127-138.

Lasserre C, Gaudemer Y, Tapponnier P, et al. Fast late Pleistocene slip rate on the Leng Long Ling segment of the Haiyuan fault, Qinghai, China. J Geophys Res, 2002,107.

Liu Gui-ping & Fu Zheng-xiang. (2001). Study on static stress triggering on Gulang earthquake by Haiyuan earthquake. Chinese Journal of Geophysics, 44(Suppl): 107-115.

Liu-Zeng, J., Y. Klinger, X. Xu, C. Lasserre, G. Chen, W. Chen, P. Tapponnier, and B. Zhang (2007). Millennial recurrence of large earthquakes on the Haiyuan fault near Songshan, Gansu Province, China, Bull. Seismol. Soc. Am. doi: 10.1785/0120050118.

Liu-Zeng, J., Y. Shao, Y. Klinger, K. Xie, D. Yuan, and Z. Lei (2015), Variability in magnitude of paleoearthquakes revealed by trenching and historical records, along the Haiyuan Fault, China,J. Geophys. Res. Solid Earth, 120, 8304–8333, doi:10.1002/2015JB012163.

Lin J., R. S. Stein, 2004. Stress triggering in thrust and subduction earthquakes and stress interaction between the southern San Andreas and nearby thrust and strike-slip faults, Journal of Geophysical Research: Solid Earth, 109: B02303.

Liu, C., Dong, P., Zhu, B., & Shi, Y. Stress shadow on the southwest portion of the Longmen Shan fault impacted the 2008 Wenchuan earthquake rupture. Journal of Geophysical Research: Solid Earth, 2018, 123(11), 9963-9981.

Liu, C., Zhu, B.J., Shi, Y.L., 2020. Do the two seismic gaps in the southwest Longmen Shan fault present the same seismic hazards? Journal of Geophysical Research: Solid Earth, 123, https://doi.org/10.1029/2019JB018160

Liu, C., & Shi, Y. (2021). Space-Time Stress Variations on the Palu-Koro Fault Impacting the 2018 Mw 7.5 Palu Earthquake and Its Seismic Hazards. Geochemistry, Geophysics, Geosystems, 22(5). https://doi.org/10.1029/2020GC009552

Mallman, E. P., & Parsons, T. (2008). A global search for stress shadows. Journal of Geophysical Research: Solid Earth, 113(B12), 1–16.

Molnar, P., & Deng, Q. D. (1984). Faulting associated with large earthquakes and the average rate of deformation in central and eastern Asia. Journal of Geophysical Research, 89(B7), 6203–6227. https://doi.org/10.1029/JB089iB07p06203

Meyer, B., Tapponnier, P., Bourjot, L., Métivier, F., Gaudemer, Y., Peltzer, G., et al. (1998). Crustal thickening in Gansu-Qinghai, lithospheric mantle subduction, and oblique, strike-slip controlled growth of the Tibet Plateau. Geophysical Journal International, 135(1), 1–47.

Nostro C., R. S. Stein, M. Cocco, et al., 1998. Two-way coupling between Vesuvius eruptions and southern Apennine earthquakes, Italy, by elastic stress transfer, Journal of Geophysical Research: Solid Earth, 103: 24487-24504.

Ou, Q., Kulikova, G., Yu, J., Elliott, Parsons, B., & Walker, R. (2020). Magnitude of the 1920 Haiyuan earthquake reestimated using seismological and geomorphological methods. Journal of Geophysical Research: Solid Earth, 125, e2019JB019244. https://doi.org/10.1029/2019JB019244

Peng, Z., Liu-Zeng, J., Deng, Y., Toda, S., 2022, Strong earthquake increases seismic hazard in Qinghai, China, Temblor, http://doi.org/10.32858/temblor.230

Peltzer, G., and P. Tapponnier (1988). Formation and evolution of strike-slip faults, rifts, and basins during the India-Asia collision: an experimental approach, J. Geophys. Res. 93, 15,085–15,117.

Reasenberg P. A., R. W. Simpson, 1992. Response of regional seismicity to the static stress change produced by the Loma Prieta earthquake, Science, 255: 1687-1690.

Richter, F. R. (1958), Elementary Seismology, W. H. Freeman, San Francisco, Calif.

Shi, F., Shao, Z., Zhan, W., et al., 2018. Numerical modelling of the shear modulus of stress state of active faults in the northeastern margin of the Tibetan plateau. Chin. J. Geophys. 61 (9), 3651–3663. https://doi.org/10.6038/cjg2018L0631

Shan, B., Xiong, X., Zheng, Y., Jin, B., Liu, C., Xie, Z., & Hsu, H. (2013). Stress changes on major faults caused by 2013 Lushan earthquake and its relationship with 2008 Wenchuan earthquake. Science China Earth Sciences, 56(7), 1169–1176.

Shan B, Xiong X, Wang R, et al (2015) Stress evolution and seismic hazard on the Maqin-Maqu segment of East Kunlun Fault zone from co-, post-and interseismic stress changes. Geophys J Int 200:244–253. https://doi.org/10.1093/gji/ggu395

Shi, Y. L., & Cao, J. L. (2008). Effective viscosity of China continental lithosphere. Earth Science Frontiers, 15(3), 82–95.

Sun Y J. Dong S W. Fan T Y, et al.3D rheological structure of the continental lithosphere beneath China and adjacent regions. Chinese J. Geophys.(in Chinese),2013,56(9):2936-2946, doi:10.6038/cjg20130908.

Stein R. S., 1999. The role of stress transfer in earthquake occurrence, Nature, 402: 605-609.

Stein, R. S. (2003), Earthquake conversations, Sci. Am, 288(1), 72– 79.

Tang, Q., and Z.Wang (1993). The 1990 Tianzhu-Jingtai M 6.2 Earthquake, Earthquake Publication House, Beijing, China (in Chinese).

Toda S., J. Lin, R. S. Stein, 2011. Using the 2011 Mw 9.0 off the Pacific coast of Tohoku Earthquake to test the Coulomb stress triggering hypothesis and to calculate faults brought closer to failure, Earth, Planets and Space, 63: 725-730.

Tapponnier, P., X. Zhiqin, F. Roger, B. Meyer, N. Arnaud, G. Wittlinger, and Y. Jingsui (2001). Oblique stepwise rise and growth of the Tibet plateau, Science 294, 1671–1677.

USGSa. https://earthquake.usgs.gov/earthquakes/eventpage/us7000g9zq/executive

USGSb. https://earthquake.usgs.gov/earthquakes/eventpage/iscgem912687/executive

USGSc. https://earthquake.usgs.gov/earthquakes/eventpage/iscgem909273/executive

Wan, Y., Shen, Z., Zeng, Y., & Sheng, S. (2007). Evolution of cumulative Coulomb failure stress in northeastern Qinghai-Xizang (Tibetan) Plateau and its effect on large earthquake occurrence. Acta Seismologica Sinica, 20(2), 117–132. https://doi.org/10.1007/s11589-007-0117-9

Wang, Q., Zhang, P.-Z., Freymueller, J. T., Bilham, R., Larson, K., Lai, X., et al. (2001). Present-day crustal deformation in China constrained by global positioning system measurements. Science, 294(5542), 574–577. https://doi.org/10.1126/science.1063647

Walter T. R., V. Acocella, M. Neri, et al., 2005. Feedback processes between magmatievents and flank movement at Mount Etna (Italy) during the 2002–2003 eruption, Journal of Geophysical Research: Solid Earth, 110: B10205.

Walter T. R., F. Amelung, 2007. Volcanic eruptions following M 9 megathrust earthquakes: Implications for the Sumatra-Andaman volcanoes, Geology, 35 (6): 539–542.

Wang M, Shen ZK. Present-Day Crustal Deformation of Continental China Derived from GPS and its Tectonic Implications. J Geophys Res Solid Earth, 2020,125:e2019JB018774.

Xiao J, and He JK. 2016. 3D Finite-Element Modeling of Earthquake Interaction and Stress Accumulation on Main Active Faults around the Northeastern Tibetan Plateau Edge in the Past 100 Years. Bulletin of the Seismological Society of America, 105 (5): 2724–2735.

Xiong, W., Chen, W., Zhao, B. et al. Insight into the 2016 Menyuan Mw 5.9 Earthquake with InSAR: A Blind Reverse Event Promoted by Historical Earthquakes. Pure Appl. Geophys. 176, 577–591 (2018).

Xu, X., Chen, W., Ma, W., Yu, G., & Chen, G. (2002). Surface Rupture of the Kunlunshan Earthquake (Ms 8.1), Northern Tibetan Plateau, China. Seismological Research Letters, 73(6), 884–892.

Yang, H., Wang, D., Guo, R., Xie, M., Zang, Y., Wang, Y., et al. (2022). Rapid report of the 8 January 2022 MS 6.9 Menyuan earthquake, Qinghai, China. *Earthquake Research Advances*, *2*(1), 100113. https://doi.org/10.1016/j.eqrea.2022.100113Tan Ying, Zhiyang Dai, Xianjie Zha, 2019. Deformation characteristics of the 2016 Mw5.9 Menyuan (China) earthquake by modeling Sentinel-1A and auxiliary data, International Journal of Remote Sensing, 41(7) :2725-2738.

Zhang, Y., X. Shan, G. Zhang, M. Zhong, Y. Zhao, S. Wen, C. Qu, and D. Zhao (2020). The 2016 Mw 5.9 Menyuan Earthquake in the Qilian Orogen, China: A Potentially Delayed Depth-Segmented Rupture Following from the 1986 w 6.0 Menyuan Earthquake, doi: 10.1785/0220190168.

Zheng W-J, Zhang P-Z, Ge W-P, et al. Late Quaternary slip rate of the South Heli Shan Fault (northern Hexi Corridor, NW China) and its implications for northeastward growth of the Tibetan Plateau. Tectonics, 2013,32:271–293.